BMES BIOMEDICAL ENGINEERING SOCIETY

ORIGINAL ARTICLE

In Vivo Material Properties of Human Common Carotid Arteries: Trends and Sex Differences

Marija Smoljkić[1,2] · Jos Vander Sloten[1] · Patrick Segers[3] · Nele Famaey[1]

Abstract

Introduction In vivo estimation of material properties of arterial tissue can provide essential insights into the development and progression of cardiovascular diseases. Furthermore, these properties can be used as an input to finite element simulations of potential medical treatments.

Materials and Methods This study uses non-invasively measured pressure, diameter and wall thickness of human common carotid arteries (CCAs) acquired in 103 healthy subjects. A non-linear optimization was performed to estimate material parameters of two different constitutive models: a phenomenological, isotropic model and a structural, anisotropic model. The effect of age, sex, body mass index and blood pressure on the parameters was investigated.

Results and Conclusion Although both material models were able to model in vivo arterial behaviour, the structural model provided more realistic results in the supra-physiological domain. The phenomenological model predicted very high deformations for pressures above the systolic level. However, the phenomenological model has fewer parameters that were shown to be more robust. This is an advantage when only the physiological domain is of interest. The effect of stiffening with age, BMI and blood pressure was present for women, but not always for men. In general, sex had the biggest effect on the mechanical properties of CCAs. Stiffening trends with age, BMI and blood pressure were present but not very strong. The intersubject variability was high. Therefore, it can be concluded that finding a representative set of parameters for a certain age or BMI group would be very challenging. Instead, for purposes of patient-specific modelling of surgical procedures, we currently advise the use of patient-specific parameters.

Keywords Human common carotid artery · Material properties · Constitutive modelling · In vivo parameter estimation

---

✉ Nele Famaey
nele.famaey@kuleuven.be

Marija Smoljkić
marija.smoljkic@fsb.hr

Jos Vander Sloten
jos.vandersloten@kuleuven.be

Patrick Segers
patrick.segers@ugent.be

1   Biomechanics Section, Mechanical Engineering Department, KU Leuven, Celestijnenlaan 300C, 3001 Heverlee, Leuven, Belgium

2   Faculty of Mechanical Engineering and Naval Architecture, University of Zagreb, Zagreb, Croatia

3   IBiTech-bioMMeda, Ghent University, Ghent, Belgium

Introduction

Cardiovascular diseases (CVDs) are the most common global cause of death and are expected to grow to more than 23.6 million per year by 2030 [1]. Many of these, e.g. heart attack or stroke, are preceded by atherosclerosis, i.e. a hardening of the arterial tissue which does not show any signs or symptoms until severe narrowing or total blockage of an artery occur. It is believed that understanding of disease progression, diagnostic process as well as the pre-operative planning and outcome prediction of cardiovascular procedures (e.g. balloon angioplasty [2] and stent placement [3]) could benefit greatly from in vivo estimation of mechanical properties of the vascular tissue. This is even more so if these mechanical properties are related to more structurally based material models such as those published by [4–6]. These models take into account contributions of elastin and collagen to the mechanical properties of the wall.

However, the fact that the amount and quality of possible in vivo measurements is limited, and that vascular tissue is anisotropic and subjected to large nonlinear deformations, makes the estimation of mechanical properties very challenging. The available 3D in vivo measurement techniques, such as echography, magnetic resonance imaging (MRI) or computed tomography (CT), are only able to provide geometrical information which in some cases includes the thickness of the arterial wall. In the 4D model, the deformation can be extracted as well. The load, i.e. intraluminal pressure, still needs to be acquired separately. This can currently be done non-invasively only for superficial arteries (e.g. common carotid artery, CCA) by applanation tonometry [7]. For non-superficial arteries, the pressure curve can be approximated from the standard auscultatory systolic and diastolic pressure measurements on the brachial artery by using a cardiovascular simulator as described in [8, 9]. The information on in vivo axial prestretch [10, 11] and circumferential residual stress [10, 12] remain unknown. Multiple groups have made attempts to estimate the material parameters in vivo [13–18]. The method published by [15] was used to estimate the mechanical properties of human abdominal aorta in [19]. They found that sex differences were more pronounced than age-related effects. [16] applied their method on non-invasive pressure-diameter data from human CCAs to compare mechanical properties of normotensive and hypertensive subjects [20]. They report, among other findings, that hypertensive subjects had a stiffer elastin-dominated matrix, despite treatment. A different approach to estimating material properties in vivo is presented in [21]. There, authors work with real geometries and use an inverse approach to obtain the material parameters by using the constitutive equations and deformation relation between the two loading states (e.g., diastolic and systolic pressures).

Our group previously published a method to estimate the material and geometrical parameters of a structural constitutive model directly from non-invasive clinical data [18]. In this study, this method is applied on a large population data set on human common carotid artery [22]. The goal is to quantify differences in mechanical properties between men and women and search for correlations of the parameters with age, body mass index, blood pressure etc. As such, the importance of patient-specific material properties can be assessed. In the following section, the employed data acquisition techniques and material parameter estimation approach are explained. Afterwards, the obtained results are reported and discussed, followed by a brief summary of the main conclusions.

Materials and Methods

Patient Data

103 subjects (76 male, 27 female) from the Asklepios study [22] were randomly selected. The study only included subjects who had no previous record of cardiovascular disease. Table 1 shows the demographics of the studied population. For all 103 subjects, the non-invasive pressure, diameter and intima-media thickness (IMT) measurements obtained in the Asklepios study were used. Outer diameter measurements, more precisely, the diameter at the media-adventitia transition, as well as the IMT were obtained from a resting echocardiographic examination on the left common carotid artery (CCA). For that purpose, arterial diameter distension waveforms were obtained using a commercially available ultrasonographic system (VIVID 7, GE Vingmed Ultrasound, Horten, Norway) equipped with a vascular transducer (12 L) set at 10 MHz. Since it is challenging to recognize the transition from the adventitia to the surrounding tissue with non-invasive imaging techniques, the media to adventitia transition was taken as the outer diameter. Diameter distension waveforms were acquired using a dedicated application that was programmed onto the Vivid 7 scanner, based on processing radio-frequency (RF) data. The RF region of interest was placed over a section of the artery, containing both the anterior and posterior walls. Within this region of interest radio-frequency data are acquired at 209 frames/s along eight evenly distributed beams. The RF data are stored together with B-mode cineloops for offline analysis, yielding diameter distension waveforms with a temporal resolution of 600 Hz. More information about the diameter measurement can be found in [23, 24]. The used measurements were averaged over at least five cardiac cycles during normal breathing. Additional technical details about the IMT measurements can be found in [25]. Pressure waveforms were acquired using applanation tonometry [7] with a Millar pentype tonometer

Table 1 Baseline characteristics of the studied population

	Men (n = 76)	Women (n = 27)
Age (y)	49.6 ± 4.4	49.4 ± 4.8
Height (cm)	174.2 ± 5.5	$161.3 \pm 4.5^*$
Weight (kg)	79.3 ± 14.6	$63.9 \pm 12.7^*$
BMI (kg/m^2)	26.1 ± 4.3	24.6 ± 4.8
DP (mmHg)	78.9 ± 10.1	75.6 ± 8.0
SP (mmHg)	134.1 ± 14.7	133.5 ± 17.1
MBP (mmHg)	97.3 ± 10.9	94.9 ± 9.8
PP (mmHg)	55.2 ± 9.8	57.9 ± 14.0
d_o^{dias} (mm)	7.8 ± 0.9	$6.7 \pm 0.8^*$
d_o^{sys} (mm)	8.4 ± 1.0	$7.1 \pm 0.8^*$
Δd (mm)	0.59 ± 0.15	$0.48 \pm 0.14^*$
IMT (mm)	0.698 ± 0.113	$0.606 \pm 0.076^*$

Reported values are means $\pm$ standard deviations

BMI body mass index, *DP* diastolic pressure, *SP* systolic pressure, *MBP* mean blood pressure, *PP* pulse pressure, d_o^{dias} diastolic outer diameter, d_o^{sys} systolic outer diameter, Δd change in diameter between systole and diastole, *IMT* intima-media thickness

$^*p < 0.05$ between men and women

(SPT 301, Millar Instruments, Houston, TX). Measurements from at least three cardiac cycles were averaged.

The diameter and pressure waveforms were not obtained simultaneously so the synchronization of the two was done in post-processing. This was performed manually in Matlab R2015a (The MathWorks, Natick, MA, USA) by matching the maximal diameter to the maximal pressure and minimizing the difference between the loading and the unloading part of the pressure-diameter curve. The user had to manually place multiple points over the pressure curve and then choose the corresponding points on the diameter curve. That defined different regions used for the synchronization (Fig. 2a). Afterwards, the synchronization was automatic and set so that the marked points on the pressure and diameter curve had to match. One example of the pressure-diameter curve before and after the synchronization is shown on Fig. 1b. One person did the synchronization of all the subjects used in this study. The unloading part of the pressure-diameter curve and the IMT were used as an input to the parameter estimation procedure.

Material Models

In this study, two hyperelastic constitutive material models were used. Hyperelastic models relate stress to strain by means of a strain energy density function (SEDF). The Mooney–Rivlin model is an isotropic phenomenological model that contains two material parameters. The Gasser–Ogden–Holzapfel (GOH) model [6] is an anisotropic structural model with five material parameters which are related to the main constituents of the arterial wall. In both cases, the arterial tissue is approximated as incompressible, so the relationship between the radial λ_r, circumferential λ_θ and axial λ_z principal stretch can be expressed as $\lambda_r \lambda_\theta \lambda_z = 1$.

Mooney–Rivlin Model

The Mooney–Rivlin (MR) SEDF is a linear combination of two invariants, I_1 and I_2, of the right Cauchy–Green deformation tensor, written as

$$\Psi = c_1(I_1 - 3) + c_2(I_2 - 3),$$
$$I_1 = \lambda_r^2 + \lambda_\theta^2 + \lambda_z^2, \qquad I_2 = \lambda_r^2\lambda_\theta^2 + \lambda_\theta^2\lambda_z^2 + \lambda_z^2\lambda_r S^2. \tag{1}$$

In the above equation, c_1 and c_2 are material constants in dimensions of stress.

Gasser–Ogden–Holzapfel Model

The GOH model additively decomposes the energy stored in the ground matrix (Ψ_{mat}) and the collagen fibre families (Ψ_{col}) as

$$\Psi = \Psi_{mat} + \Psi_{col}. \tag{2}$$

The model also accounts for dispersion of the collagen fibres. To describe the isotropic behaviour of the ground matrix, the Neo-Hookean material model is used, as

$$\Psi_{mat} = \frac{\mu}{2}(I_1 - 3), \tag{3}$$

where I_1 is the same as in Eq. 1 and μ is the stiffness of the ground matrix in dimensions of stress.

The anisotropy comes from two collagen fibre families embedded in the ground matrix. The SEDF related to their contribution is given as

$$\Psi_{col} = \frac{k_1}{2k_2} \sum_{i=4,6} \left\{ \exp\left\{k_2[(\kappa I_1 + (1-3\kappa)I_i) - 1]^2\right\} - 1 \right\},$$
$$I_{4,6} = \lambda_z^2\sin^2\alpha + \lambda_\theta^2\cos^2\alpha, \tag{4}$$

where $I_{4,6}$ are invariants equal to the square of the stretch in the directions of collagen fibres. The families are assumed to be symmetric w.r.t. the circumferential direction. Their orientation is described with angle α and $-\alpha$ for the first and the second fibre family, respectively. If the fibre families are symmetrical, as it is assumed in this study, and the shear is negligible, these two invariants are identical. The stiffness of the collagen fibres k_1 is a stress-like parameter. k_2 is dimensionless and is related to the stiffening effect of the fibres in the higher pressure domain. A simplified version of the model is used for the limit cases when $k_2 = 0$ as proposed by [26]:

$$\Psi = \frac{\mu}{2}(I_1 - 3) + \frac{k_1}{2}\sum_{i=4,6}(I_i - 1)^2. \tag{5}$$

The GOH model takes into account the dispersion of the fibres about the direction α by introducing an additional parameter κ. κ can range between 0 and 1/3 for the cases with no dispersion and isotropic dispersion, respectively. Ψ_{col} contributes to the total SEDF only in tension, so when $I_{4,6} > 0$. When the fibres are compressed, the response of the tissue comes only from the ground matrix and is purely isotropic [27].

Parameter Identification

Parameter identification was performed according to the approach published in [18] and further used in [28, 29]. The artery was considered stress-free when the intraluminal pressure is zero and there is no axial prestretch, i.e. the artery is a closed cylinder. In short, the measured diameter and the in vivo loaded wall thickness were used as an input to the optimization procedure. The difference between the measured pressures P^{exp} and pressures predicted by a model P^{mod}, assuming either MR or GOH material, was minimized in

Fig. 1 a Different regions defined on the pressure and the diameter curve used for the synchronization, and the corresponding loading and unloading separation. The unloading part of the curve is used as an input into the model; **b** Original pressure-diameter curve before synchronization (black full line), and the loading (red dotted line) and the unloading (blue dotted line) curve after the synchronization
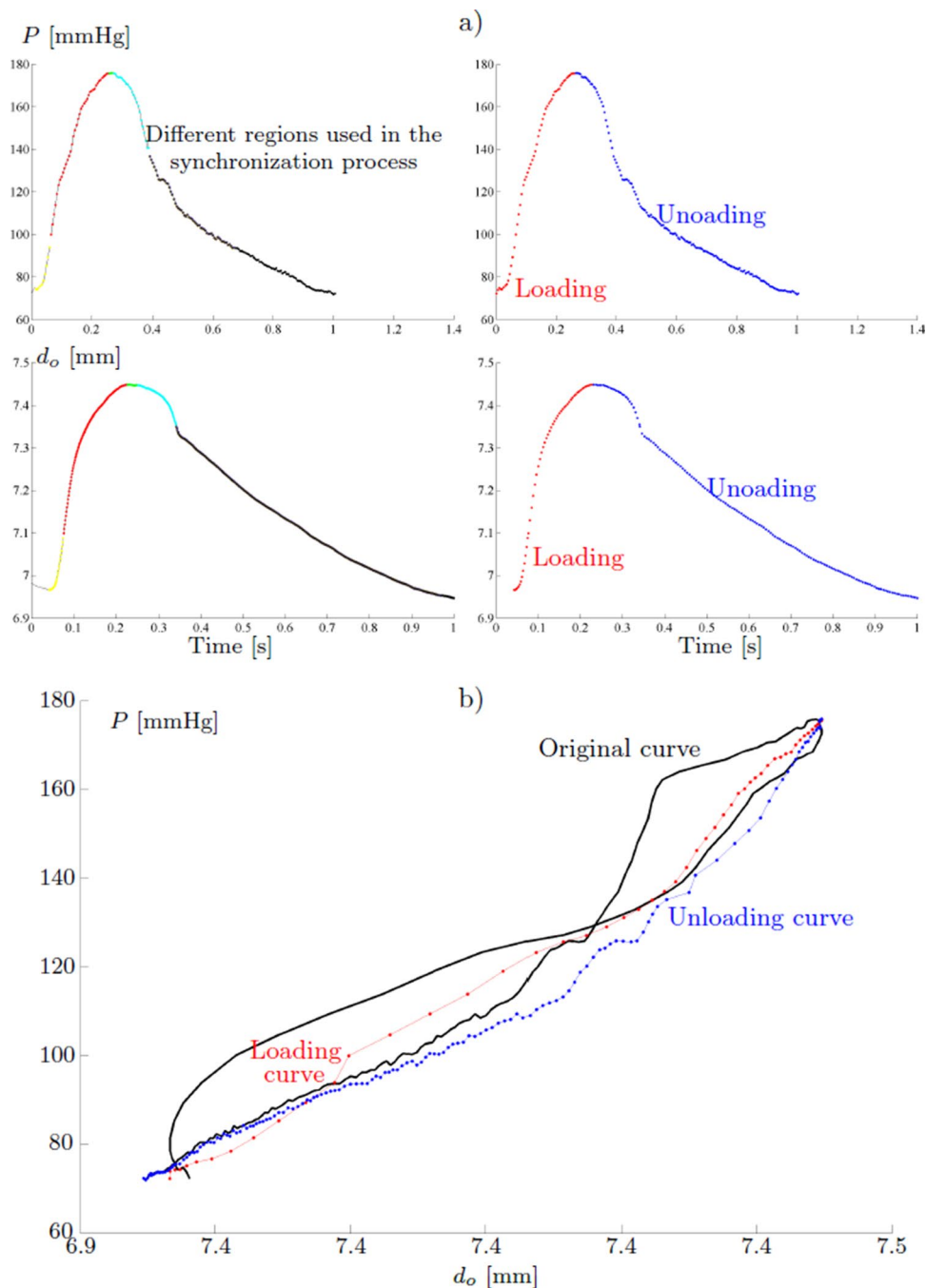
Matlab R2015a (The MathWorks, Natick, MA, USA). The model pressures can be calculated as

$$P_j^{mod} = \int_{\lambda_o}^{\lambda_i} \left(\lambda_\theta^2 \lambda_z - 1\right)^{-1} \frac{\partial \Psi}{\partial \lambda_\theta} d\lambda_\theta. \tag{6}$$

The circumferential stretch (ratio of the loaded to the unloaded radius) at the inner and the outer wall is denoted with λ_i and λ_o, respectively. j represents a certain data record both for the measured pressure curve and for the corresponding reduced axial force. The output of the optimization were

the material parameters of each model and additional geometrical parameters, i.e. the wall thickness in unloaded configuration H and the axial prestretch λ_z. The circumferential residual stresses were not taken into account.

Ideally, the optimization process would include the minimization between the measured reduced axial force (i.e. the force acting on the arterial tissue in the axial direction) and the same force predicted by a constitutive model,
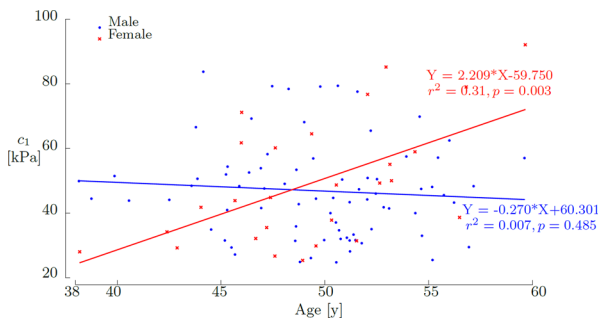
Fig. 2 Stiffness parameter c_1 in relation to age for men (blue dots) and women (red x)

$$F_j^{mod} = \pi \rho_i^2 \left(\lambda_i^2 \lambda_z - 1\right) \int_{\lambda_o}^{\lambda_i} \left(\lambda_\theta^2 \lambda_z - 1\right)^{-2} \left(2\lambda_z \frac{\partial \Psi}{\partial \lambda_z} - \lambda \frac{\partial \Psi}{\partial \lambda_\theta}\right) \lambda_\theta d\lambda_\theta, \tag{7}$$

where ρ_i is the inner radius in the unloaded configuration. However, measuring the reduced axial force in vivo is impossible, which is why an assumption is introduced, namely that this force remains approximately constant in the physiological pressure range [30].

To assure a good parameter estimation, two additional assumptions had to be introduced. Both of them are related to the strain energy of the arterial wall. First one ensures that the energy across the wall remains approximately constant at diastolic pressure. The second one compares the strain energy of the ground matrix and the strain energy of the collagen fibre families at diastolic pressure and makes sure that the latter contributes more. This condition was derived from studies performed on animals and humans by [31, 32]. Minimization of the difference in pressures and the assumption related to the reduced axial force and strain energy yield the following objective function:

$$\varepsilon(pars) = \sum_{j=1}^{n} \left\{ \left[w_p \left(P_j^{mod} - P_j^{exp}\right) \right]^2 \right.$$
$$+ \left[w_f \left(\frac{F_j^{mod}}{A_j^{mod}} - \frac{F^{average}}{A_j^{mod}}\right) \right]^2 \right\}$$
$$+ \sum_{k=1}^{m} \left\{ \left[w_{\Psi_1} \left(\Psi_k^{dias,mod} - \Psi^{average}\right) \right]^2 \right.$$
$$+ \left[w_{\Psi_2} \left(\Psi_{k,col}^{dias,mod} - \Psi_{k,mat}^{dias,mod}\right) \right]^2 \right\}. \tag{8}$$

In the above equation, *pars* represents a vector of optimized parameters. A zero order polynomial was fitted to $\boldsymbol{F}^{mod}$ (*polyfit* function in Matlab®) to calculate $F^{average}$. A_j^{mod} stands for the current cross sectional area of the arterial wall and is calculated as

$$A_j^{mod} = \pi \left[\left(R_o \lambda_{o,j}\right)^2 - \left(R_i \lambda_{i,j}\right)^2\right]. \tag{9}$$

$\Psi_k^{dias,mod}$ is the strain energy density at diastole across the wall thickness. k represents different points throughout the wall thickness going from 1 to m, m is the number of points defined through the arterial wall thickness for purposes of numerical integration and is set to 11 in our case. The *polyfit* function was used once again but now on $\Psi^{dias,mod}$ to calculate $\Psi^{average}$. $\Psi_{k,mat}^{dias,mod}$ and $\Psi_{k,col}^{dias,mod}$ are the energy contributions from the ground matrix and fibre families respectively, at diastolic pressure. The weighting factors depend on the chosen units and were set to 1 for w_p, 10^{-2} for w_f, 10^{-4} for w_{Ψ_1} and 10^{-1} for w_{Ψ_2} in this study.

When the MR model was used, the last part in Eq. 8 is omitted, since the model is not able to distinguish between the collagen and matrix contribution.

As mentioned earlier, besides material model parameters, additional geometrical parameters were fitted. The upper and lower boundary were set for each parameter. For parameters c_1 and c_2 in case of MR and μ and k_1 in case of GOH the boundaries were between 0 and 1000 kPa. k_2 ranged between 0 and 50, α between 0 and 90° and κ between 0 and 1/3. These boundaries were set as suggested in [6]. The boundaries of the geometrical parameters were adapted for each subject. For H, the lower boundary was equal to the patient's IMT and the upper boundary was set to 3xIMT. In the case of axial prestretch λ_z, the boundaries were taken from [33]. They measured the ex vivo λ_z on the CCA of 365 cadavers and found a correlation between λ_z and age. The upper and lower boundaries were set to the reported 95% prediction interval. The uniqueness of parameters was checked by perturbing the initial guesses for every case. Five out of 20 minimization results resulted in the same material parameters and an equal fitting error. They all retrieved what we believe to be the global minimum. Other sets, if converged, gave different values for parameters but also resulted in bigger residuals, meaning they converged to a local minimum and were not taken into account.

Statistics

The values are reported as means and standard deviations. Two-sample t-tests were performed to compare differences in baseline characteristics, listed in Table 1, between female and male participants. Linear regression was used to see the relationship between the material parameters and the independent variables such as age, BMI, etc. Pearson correlation coefficient r^2 an the corresponding p-values are reported to quantify a trend and its significance. A p-value less than 0.05 was considered significant. The statistical tests were performed in Matlab®R2015a.

Table 2 Correlations between Mooney–Rivlin model parameters c_1 and c_2 and different independent variables

F - r^2/p M - r^2/p	Age	BMI	d_{dias}	d_{sys}	Δd
c_1	↑ **0.31/0.003** 0.01/0.485	↑ **0.24/0.010** ↑ **0.06/0.042**	↑ **0.28/0.005** ↑ *0.05/0.056*	↑ **0.19/0.024** 0.03/0.146	↓ *0.13/0.063* ↓ **0.06/0.030**
c_2	↑ **0.30/0.003** ↑ *0.04/0.093*	↑ *0.14/0.060* 0.03/0.111	↑ **0.27/0.006** 0.03/0.171	↑ **0.18/0.026** 0.01/0.420	↓ *0.12/0.073* ↓ **0.14/0.001**
	IMT	DP	SP	MBP	PP
c_1	↓ *0.14/0.054* ↓ **0.17/0.000**	0.06/0.224 ↑ **0.11/0.004**	↑ **0.28/0.005** ↑ **0.21/0.000**	↑ **0.19/0.022** ↑ **0.16/0.000**	↑ **0.26/0.007** ↑ **0.12/0.002**
c_2	↓ **0.16/0.036** ↓ **0.16/0.000**	0.02/0.486 ↑ **0.13/0.001**	↑ **0.17/0.031** ↑ **0.23/0.000**	0.10/0.108 ↑ **0.19/0.000**	↑ **0.18/0.027** ↑ **0.12/0.003**

The results are reported as correlation coefficient over p-value (r^2/p) for women (F, upper row) and men (M, lower row) separately. The arrows indicate an increasing (↑) or decreasing (↓) trend. Significant correlations are marked in bold ($p < 0.05$) or italic ($p < 0.10$)

Results

As visible in Table 1, men had larger CCA diameters (d_{dias}, d_{sys}) and change between the systolic and diastolic diameter (Δd), as well as a thicker arterial wall (IMT), $p < 0.05$. There was no significant difference in blood pressures.

Mooney–Rivlin

In the case of the MR model, the average goodness of fit evaluated with the coefficient of determination R^2 was 0.96. In most of the cases the model was able to capture the mechanical behaviour of the CCA, the range of the R^2 being between 0.87 and 0.99.

Figure 2 shows the stiffness c_1 in relation with age, both for men and women. The c_1 increases with age in women ($r^2 = 0.31$, $p < 0.05$) but no trend was present for men. However, there was no significant difference in the values of c_1 between men and women, 46.9 ± 14.7 and 49.3 ± 19.5 kPa, respectively.

Table 2 reports correlation coefficients and significance levels of MR material parameters c_1 and c_2 with age, BMI, diastolic (d_{dias}) and systolic (d_{sys}) diameter, difference between systolic and diastolic diameter (Δd), IMT, diastolic (DP) and systolic (SP) pressure, mean blood pressure (MBP) and pulse pressure (PP). In general, the difference in men and women is quite pronounced. Both c_1 and c_2 increased with age, BMI, d_{dias}, d_{sys}, SP and PP for women. For men, only an increase with BMI and different pressure measurements (DP, SP, MBP and PP) was present for c_1, while a decreasing trend with Δd and IMT was observed. However, the correlations were quite weak (the highest r^2-value was 0.31). For men, c_2 increased with age, DP, SP, MBP and PP while it decreased with Δd and IMT. As for c_1, there was no

significant difference in the values of c_2 between men and women, 33.6 ± 10.3 and 35.8 ± 13.3 kPa, respectively.

In the case of the geometrical parameter H (the thickness in the unloaded configuration), there was a significant difference between men (0.83 ± 0.14 mm) and women (0.71 ± 0.10 mm). Axial prestretch λ_z was similar for men and women, 1.19 ± 0.11 and 1.18 ± 0.10 respectively. Best-fit values of the model parameters were used to calculate the reduced axial force that acts on the arterial tissue in the axial direction ($F_{average}$ in Eq. 8). On average, men had higher estimated $F_{average}$ than women (1.36 ± 0.99 N vs. 1.03 ± 0.82 N) but the difference was not statistically significant.

Gasser–Ogden–Holzapfel

The GOH model always resulted in high R^2-values, ranging between 0.94 and 0.99.

Table 3 reports correlation coefficients and significance levels of three GOH material parameters μ, k_1 and k_2 with all the independent variables (age, BMI, d_{dias}, d_{sys}, Δd, IMT, DP, SP, MBP and PP). Since the tissue was modelled as a single layer (no separation between the intima and media), the parameters α and κ and their correlations are not reported. In Table 3, less trends could be observed than with the MR parameters. The difference in males and females is however still present.

The stiffness of the matrix material μ weakly increased with age and decreased with IMT for men while no trends were present for women. No trends were present for the stiffness of the collagen fibres k_1 in either men or women. Concerning the parameter k_2, an increasing trend with BMI was observed for women ($r^2 = 0.42$, $p = 0.001$, see also Fig. 3). No significant correlations were obtained for any of the other variables for women. In the case of men, only weak decreasing trends of k_2 with Δd, DP and MBP were observed.

Table 3 Correlations between GOH model parameters μ, k_1 and k_2 and different independent variables

F - r^2/p M - r^2/p	Age	BMI	d_{dias}	d_{sys}	Δd
μ	0.01/0.697	0.04/0.356	0.09/0.130	0.09/0.145	0.00/0.799
	0.03/0.159	↑ **0.06/0.041**	0.00/0.589	0.01/0.467	0.03/0.112
k_1	0.02/0.446	0.01/0.720	0.00/0.790	0.00/0.752	0.01/0.697
	0.02/0.265	0.00/0.647	0.01/0.564	0.01/0.425	↓ *0.05/0.064*
k_2	0.03/0.475	↑ **0.42/0.001**	0.10/0.136	0.08/0.183	0.00/0.792
	0.02/0.209	0.01/0.532	0.02/0.291	0.02/0.207	↓ **0.06/0.047**
	IMT	DP	SP	MBP	PP
μ	0.08/0.156	0.01/0.709	0.01/0.737	0.00/0.993	0.02/0.519
	↓ **0.06/0.034**	0.01/0.451	0.00/0.939	0.00/0.617	0.01/0.509
k_1	0.02/0.478	0.01/0.609	0.00/0.905	0.01/0.734	0.00/0.881
	0.03/0.118	0.00/0.675	0.01/0.512	0.00/0.579	0.00/0.583
k_2	0.04/0.386	0.02/0.535	0.06/0.252	0.01/0.746	↓ *0.15/0.065*
	0.03/0.172	↓ **0.10/0.006**	0.03/0.154	↓ **0.08/0.019**	0.01/0.534

The results are reported as correlation coefficient over p-value (r^2/p) for women (F, upper row) and men (M, lower row) separately. The arrows indicate an increasing (↑) or decreasing (↓) trend. Significant correlations are marked in bold ($p < 0.05$) or italic ($p < 0.10$)
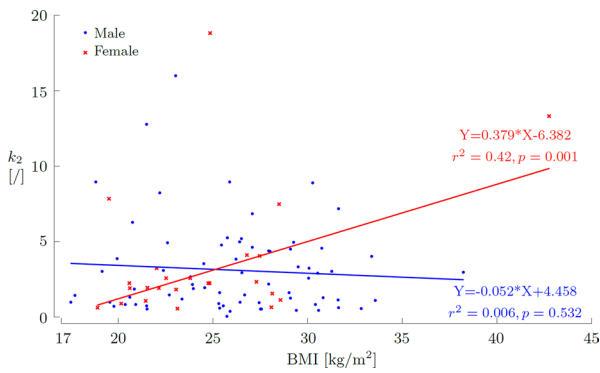

Fig. 3 k_2 in relation to BMI for men (blue dots) and women (red x)

Table 4 Average values $\pm$ their standard deviations of the fitted GOH material and geometrical parameters for men and women

	Men	Women
μ (kPa)	19.6 ± 12.5	26.6 ± 43.6
k_1 (kPa)	93.6 ± 177.1	105.7 ± 214.0
k_2 (–)	3.10 ± 3.00	3.62 ± 4.33
α (°)	46.1 ± 31.0	50.9 ± 28.2
κ (–)	0.135 ± 0.142	0.099 ± 0.129
H (mm)	1.25 ± 0.46	$1.01 \pm 0.27^*$
λ_z (–)	1.20 ± 0.11	1.15 ± 0.11

$^*p < 0.05$ between men and women

Table 4 reports average values of GOH material parameters for men and women separately. In general, women had higher values of all parameters related to stiffness (μ, k_1 and k_2) but again these differences were not significant. The unloaded thickness H was significantly higher for men and there was no significant difference in λ_z. As with the MR parameters, best-fit values of the model parameters were used to calculate $F^{average}$ (Eq. 8). The obtained values were in general lower than the ones obtained with MR model and were lower for men than for women (0.23 ± 0.17 N vs. 0.52 ± 1.96 N). This difference was not significant.

Mooney–Rivlin vs. Gasser–Ogden–Holzapfel

On Fig. 4, two representative pressure-diameter curves were shown together with their corresponding GOH and MR model fits. A case where both models gave a good fit is shown on the upper plot. Below, a case where MR does not provide an ideal fit and linearizes the observed behavior is demonstrated. Not surprisingly, this happens for cases when a subject has more pronounced nonlinearity.

To compare the performance of the models, predictions of the pressure-diameter curve were plotted for 0–27 kPa pressure range, which also included pressures below and above the physiological range (see Fig. 5). This was done for one subject (male, 38.7 years) for whom the GOH material parameters resulted in the lowest root mean square error with respect to the average parameters. Average parameters were calculated by averaging the fitted parameters, not by fitting the average pressure-diameter curve. Table 5 shows the average parameters for each model, GOH and MR, and patient-specific parameters from the mentioned subject. Additionally, the root-mean-square errors (RMSE) are reported between the average and the patient-specific parameters. The reported patient-specific parameters were used to obtain the results shown on Fig. 5.

Table 5 Average values of parameters for GOH and MR model, patient-specific values for a specific subject, and the RMSE difference between them

	GOH average	GOH specific		MR average	MR specific
μ (kPa)	21.4	19.9	c_1 [kPa]	47.55	44.48
k_1 (kPa)	96.8	81.6	c_2 [kPa]	34.14	26.64
k_2 (–)	2.98	2.57	H [mm]	0.80	0.77
α (°)	9.35	50.9	λ_z [–]	1.18	1.29
κ (–)	0.125	0.330			
H (mm)	1.19	0.98			
λ_z (–)	1.29	1.27			
RMSE	15.49		RMSE	3.06	

The patient-specific parameters were used to obtain the results shown on Fig. 5
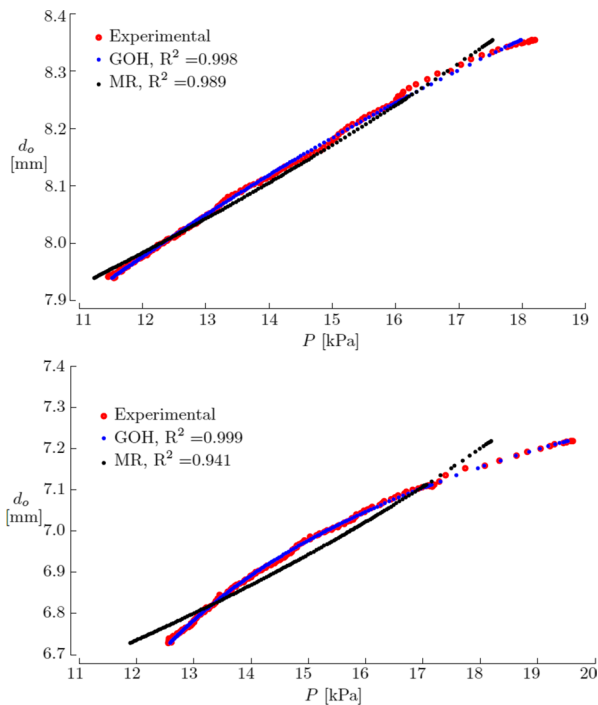
Fig. 4 Two representative pressure-diameter curves (Experimental) and their corresponding Gasser–Ogden–Holzapfel (GOH) and Mooney–Rivlin (MR) fits

Fig. 5 Comparison of pressure-diameter curves predicted by the Mooney–Rivlin (red dotted line) and the GOH (blue circles) model for one male subject (38.7 years) for pressures between 0 and 27 kPa (0 and 200 mmHg). Pressure 10.8 kPa corresponds to the subject's diastolic and 19.6 kPa to the systolic pressure

Discussion

This study estimated in vivo material properties of human CCAs (n = 103) from non-invasively obtained pressure, diameter and wall thickness measurements obtained as a part of the Asklepios study [22]. The parameters were estimated by minimizing the difference between the measured pressure and that predicted by the material model, and by adding additional conditions related to the strain energy and the reduced axial force as proposed in [18]. The two material models used in this study describe the artery as a nonlinear, passive, incompressible, one-layer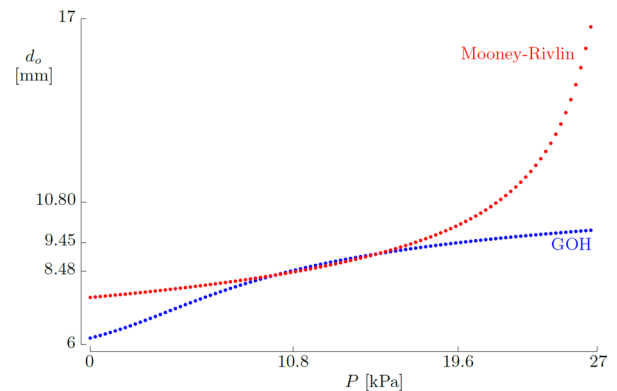ed tissue. Additionally, the GOH model describes the tissue as anisotropic. The axial prestretch is taken into account, while the residual circumferential stress is disregarded. The latter can induce an underestimation of the tissue's stiffness (reflected in lower values of parameters μ, k_1 and k_2 in the GOH model, and c_1 and c_2 in the MR model). However, based on our previous studies on simulated data, this effect was not major [18]. To avoid over-parameterization, it was chosen not to include the opening angle as additional geometrical parameter.

Both the MR and the GOH model were able to capture the tissue's behaviour which is reflected in high R^2-values (0.87–0.99 for MR, 0.94–0.99 for GOH). Furthermore, both of them showed high robustness to a change in the initial input parameters, since different inputs resulted in similar outputs. It is important to note that the obtained parameters are considered to be phenomenological since the artery is modelled as a single-layer, i.e. no distinction was made between the intima and the media. The adventitia was not taken into account since the media to adventitia transition has been taken as the outer diameter, due to the limitations of the currently available non-invasive imaging techniques.

Modelling the artery as a three-layered structure would be beneficial, however it would also increase the number of fitting parameters and jeopardize their uniqueness.

Variability is present in the data and it is very difficult to infer the difference between patient variability and measurement variability. Both will be present in the total variability, though great care was taken in the Asklepios study to standardize the applied measurement protocols, as well as the subsequent post-processing steps. One should also be aware of the fact that the resulting parameter uncertainty will also propagate into subsequent numerical simulations made with these parameters. Ideally, uncertainty quantification techniques are adopted to this end, e.g. by using a Gaussian emulator machine [34].

Effects of Age, BMI and Blood Pressure

For the obtained parameters, the effect of ageing, sex, increased BMI, blood pressure, wall thickness and diastolic to systolic diameter change was studied. The effects were more pronounced for the MR parameters than for the GOH ones.

Many in vivo studies investigated age-related changes in arteries and reported stiffening effect of age on the arterial response [19, 20, 35–37]. In our dataset, the arteries were stiffer with age for women when looking at parameters c_1 and c_2, while the trend was less pronounced for men. In the case of the GOH parameters, women on average had higher values of stiffness parameters related to elastin (μ) and collagen (k_1 and k_2) than men, although these differences were not statistically significant. Also, no correlation of μ, k_1 and k_1 with age was found either for men or women. This can be explained by the small age range of the subjects included in this study (35–55). Other studies included a bigger age range, e.g. [20] studied subjects between 21 and 69 years. Additionally, they had two groups of subjects, normotensive and hypertensive. In their case, age was positively correlated with residual stresses and altered fibrillar collagen in normotensive subjects, and hypertensive subjects had higher levels of stresses, increased smooth muscle tone, and a stiffer elastin-dominated matrix despite treatment. Linearized stiffness was previously calculated on the Asklepios data set by [37]. They concluded that stiffening with age was present for both men and women and a significant age–sex interaction was found indicating that stiffening occurred at a faster pace in women. For that reason, it is not surprising that in our subset females also had stiffer arteries than males. We expect that the effect of stiffening with age for men would be present if an extended data set were used.

Different studies already reported a stiffening effect of increased weight or BMI on arteries. [38] reported that pulse wave velocity was significantly increased in 27 obese patients in comparison with 25 non-obese patients participating in the study. In [39], the aortic pulse-wave velocity was strongly correlated with a higher BMI and body weight. The study involved 363 participants. [40] measured properties of the carotid, femoral and brachial arteries in 1306 individuals and concluded that carotid distensibility decreased with BMI both in men and women and the effect was more evident for younger subjects (up to 40 years). In our study, an increase in BMI also had a significant effect on the stiffness of the arterial tissue. For women, this was reflected through parameter c_1 ($r^2 = 0.24$) and for men through parameter c_2 ($r^2 = 0.11$) for the MR model. The GOH parameter k_2 increased with higher BMI for women ($r^2 = 0.42$) but not for men.

As expected, blood pressure (BP) also played an important role in the tissue response, making it less compliant for an increasing BP. This was confirmed for different BP measurements (see effect of DP, SP, MBP and PP on c_1 and c_2 in Table 2). However, there was almost no effect on GOH parameters and in case of k_2, the values surprisingly even slightly decreased with increasing diastolic (DP) and mean (MBP) blood pressure (Table 3). [20] reported an increased stiffness of matrix material μ in CCAs of hypertensive (37.74 ± 7.77) subjects compared to normotensive (31.32 ± 5.14) subjects. This trend was not present in our study, although the reported values of μ were in the same order of magnitude as ours.

IMT is considered as an important predictor of CVDs. Carotid IMT, together with aortic calcification, is reported as predictor of stroke [41]. The remodelling of the arterial wall by increasing its thickness reduces and normalizes the wall stress. A study performed by [42] reported that as the IMT increases after menopause in women, the elasticity of the CCA increases as well, thus the stiffness decreases. Both for men and women, c_1 and c_2 decreased with increasing IMT in this study, while there was no effect on μ, k_1 and k_2 GOH parameters.

Overall, sex had the biggest effect on the mechanical properties of CCAs. On average, women had a higher stiffening rate of the MR parameters c_1 and c_2 w.r.t. age, BMI and blood pressure than men. In case of the GOH model, BMI had a significant effect on k_2 in women while no effect on men. A study performed by [37] on 2195 subjects from the Asklepios study reported similar findings. They evaluated local arterial stiffness of CCA by means of compliance and distensibility coefficients, local pulse wave velocity and the characteristic impedance. All but the compliance coefficient showed a higher stiffening rate in women than in men.

Mooney–Rivlin vs. Gasser–Ogden–Holzapfel

The pressure-diameter curves on Fig. 5 start from a different diameter at zero pressure due to the fact that the models predict different unloaded configurations. The models

Fig. 6 Sensitivity of the objective function T_{fun} (which includes pressures and forces) on the parameters
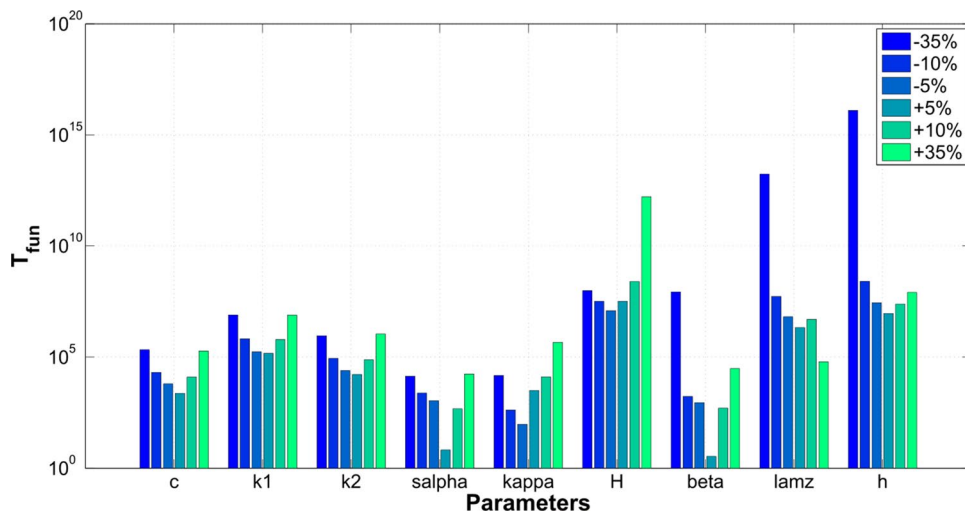

also show a quite distinct difference in curvature. The GOH model predicts a stiffer (which we believe to be more realistic) response in the supra-physiological domain which is of big importance for pre-operative scenarios and surgical outcome predictions. The MR response will, most likely, result in an overestimated deformation. This shows that even though GOH has more parameters who's structural meaning is questionable, especially when modelled as a single-layered structure, it still results in the more realistic response than the simpler, phenomenological MR model. The obtained parameters should not be interpreted as patient characteristics with a clear physical meaning, but rather as a quantitative way to compare different datasets. The GOH model is well-known in the biomechanics modelling community, its parameters are intuitive to interpret, and can be used for subsequent modelling purposes. It is important to stress that for any model, the parameters are only valid for the range in which the data is fitted. With this one example we go above this range to illustrate how different the results can be once you exceed this range.

Conclusion

This study estimated passive mechanical properties of human CCAs. This was based on the non-invasive pressure and diameter measurements of 103 healthy subjects who were participating in the Asklepios study. Two constitutive material models, MR and GOH, were used to describe the arterial behaviour. In general, the GOH model resulted in a better goodness of fit, which is not surprising considering its exponential relation which has a big effect on the predictions of deformation in the supra-physiological domain. Preference is given to the anisotropic GOH model, due to more realistic deformations at higher pressures. The advantage of the MR model lies mainly in the low number of parameters which simplifies their in vivo estimation.

In the ideal scenario, material properties could be estimated based on factors such as sex, age and BMI or a representative parameter set could be used for a predefined patient

Fig. 7 Sensitivity index for each parameter
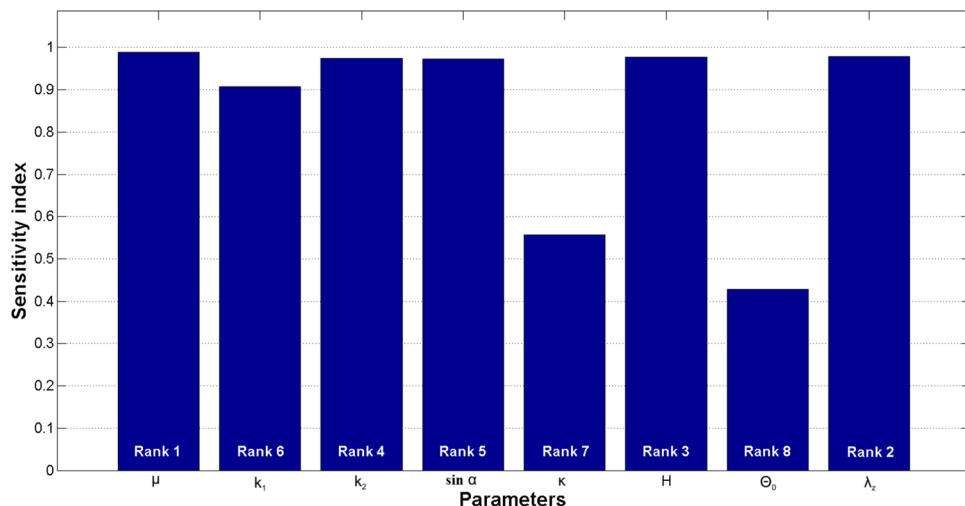
group. For that reason, the effect of sex, age, BMI and blood pressure on stiffness of arteries was investigated. Overall, the sex differences were pronounced, as women had a higher stiffening rate than men. The lack or weakness of trends and big inter-subject variability pointed out the importance of patient-specific parameters.

Appendix

Previously, a sensitivity analysis was performed to possibly exclude some of the material parameters. The result of it is visible on Figs. 6 and 7.

On Fig. 6, each parameter was changed for ± 5, ± 10 and $\pm 35\%$ from the actual value to see the influence on the objective function (T_{fun}, in this case the objective function included pressures and forces).

To calculate the sensitivity index (SI) shown on Fig. 7, the following analysis has been performed:

1. Each parameter was changed from the lower to the upper boundary in steps (e.g. parameter μ was changed from 0 to 1000 kPa with steps of 5).
2. For these sets of parameters, the prediction of the model in terms of diastolic pressure was calculated.
3. Based on this, a sensitivity index was calculated as follows:

$$SI = \frac{P_{max} - P_{min}}{P_{max}}. \tag{10}$$

4. Finally, all parameters with a sensitivity index higher than 0.5 were retained.

Data Availability There is no additional data or material available.

Code Availability Custom code developed in Matlab®was used (not publicly available).

Declarations

Conflict of interest The authors declare that they have no conflict of interest.

Ethical Approval No additional ethical approval was necessary for this study. The data was available from the Asklepios study for which the ethical committee of the Ghent University Hospital (Belgium) approved the study protocol and all the involved subjects gave written informed consent.

Consent to Participate All the involved subjects gave written informed consent.

Consent for Publication The authors hereby consent to publication of the work in Cardiovascular Engineering and Technology journal.

References

1. Mozaffarian, D., E. J. Benjamin, A. S. Go, D. K. Arnett, M. J. Blaha, M. Cushman, S. de Ferranti, J.-P. Després, H. J. Fullerton, V. J. Howard, M. D. Huffman, S. E. Judd, B. M. Kissela, D. T. Lackland, J. H. Lichtman, L. D. Lisabeth, S. Liu, R. H. Mackey, D. B. Matchar, D. K. McGuire, E. R. Mohler, C. S. Moy, P. Muntner, M. E. Mussolino, K. Nasir, R. W. Neumar, G. Nichol, L. Palaniappan, D. K. Pandey, M. J. Reeves, C. J. Rodriguez, P. D. Sorlie, J. Stein, A. Towfighi, T. N. Turan, S. S. Virani, J. Z. Willey, D. Woo, R. W. Yeh, and M. B. Turner. Heart disease and stroke statistics—2015 update. *Circulation*. 131(4):e29–e322, 2015. https://doi.org/10.1161/CIR.0000000000000152.
2. Badel, P., S. Avril, M. A. Sutton, and S. M. Lessner. Numerical simulation of arterial dissection during balloon angioplasty of atherosclerotic coronary arteries. *J. Biomech.* 47(4):878–889, sI: Plaque Mechanics, 2014. https://doi.org/10.1016/j.jbiomech.2014.01.009.
3. Bock, S. D., F. Iannaccone, G. D. Santis, M. D. Beule, D. V. Loo, D. Devos, F. Vermassen, P. Segers, and B. Verhegghe. Virtual evaluation of stent graft deployment: a validated modeling and simulation study. *J. Mech. Behav. Biomed. Mater.* 13:129–139, 2012. https://doi.org/10.1016/j.jmbbm.2012.04.021.
4. Holzapfel, G. A., T. C. Gasser, and R. W. Ogden. A new constitutive framework for arterial wall mechanics and a comparative study of material models. *J. Elast. Phys. Sci. Solids*. 61:1–48, 2000. https://doi.org/10.1023/A:1010835316564.
5. Zulliger, M. A., P. Fridez, K. Hayashi, and N. Stergiopulos. A strain energy function for arteries accounting for wall composition and structure. *J. Biomech.* 37:989–1000, 2004. https://doi.org/10.1016/j.jbiomech.2003.11.026.
6. Gasser, T. C., R. W. Ogden, and G. A. Holzapfel. Hyperelastic modelling of arterial layers with distributed collagen fibre orientations. *J. R. Soc. Interface*. 3(6):15–35, 2006. https://doi.org/10.1098/rsif.2005.0073.
7. Segers, P., E. Rietzschel, S. Heireman, M. D. Buyzere, T. Gillebert, P. Verdonck, and L. V. Bortel. Carotid tonometry versus synthesized aorta pressure waves for the estimation of central systolic blood pressure and augmentation index. *Am. J. Hypertens.* 18(9):1168–1173, 2005. https://doi.org/10.1016/j.amjhyper.2005.04.005.
8. Ferrari, G., M. Kozarski, K. Zieliński, L. Fresiello, A. Di Molfetta, K. Górczyńska, K. J. Pałko, and M. Darowski. A modular computational circulatory model applicable to VAD testing and training. *J. Artif. Organs*. 15(1):32–43, 2012. https://doi.org/10.1007/s10047-011-0606-4.
9. Fresiello, L., K. Zieliński, S. Jacobs, A. Di Molfetta, K. J. Pałko, F. Bernini, M. Martin, P. Claus, G. Ferrari, M. G. Trivella, K. Górczyńska, M. Darowski, B. Meyns, and M. Kozarski. Reproduction of continuous flow left ventricular assist device experimental data by means of a hybrid cardiovascular model with baroreflex control. *Artif. Organs*. 38(6):456–468, 2014. https://doi.org/10.1111/aor.12178.

10. Cardamone, L., A. Valentín, J. F. Eberth, and J. D. Humphrey. Origin of axial prestretch and residual stress in arteries. *Biomech. Model. Mechanobiol.* 8(6):431–446, 2009. https://doi.org/10.1007/s10237-008-0146-x.

11. Horny, L., T. Adamek, and M. Kulvajtova. Analysis of axial prestretch in the abdominal aorta with reference to post mortem interval and degree of atherosclerosis. *J. Mech. Behav. Biomed. Mater.* 33:93–98, 2014. https://doi.org/10.1016/j.jmbbm.2013.01.033.

12. Chuong, C. J., and Y. C. Fung. Residual stress in arteries. In: Frontiers in biomechanics, part II, edited by G. W. Schmid-Schönbein, S.L.-Y. Woo, and B. W. Zweifach. New York: Springer, 1986, pp. 117–129.

13. Schulze-Bauer, C. A. J., and G. A. Holzapfel. Determination of constitutive equations for human arteries from clinical data. *J. Biomech.* 36(2):165–169, 2003.

14. Stålhand, J., and A. Klarbring. Aorta in vivo parameter identification using an axial force constraint. *Biomech. Model. Mechanobiol.* 3(4):191–199, 2005. https://doi.org/10.1007/s10237-004-0057-4.

15. Stålhand, J. Determination of human arterial wall parameters from clinical data. *Biomech. Model. Mechanobiol.* 8(2):141–148, 2009. https://doi.org/10.1007/s10237-008-0124-3.

16. Masson, I., P. Boutouyrie, S. Laurent, J. D. Humphrey, and M. Zidi. Characterization of arterial wall mechanical behavior and stresses from human clinical data. *J. Biomech.* 41(12):2618–2627, 2008. https://doi.org/10.1016/j.jbiomech.2008.06.022.

17. Wittek, A., K. Karatolios, P. Bihari, T. Schmitz-Rixen, R. Moosdorf, S. Vogt, and C. Blase. In vivo determination of elastic properties of the human aorta based on 4D ultrasound data. *J. Mech. Behav. Biomed. Mater.* 27:167–183, 2013. https://doi.org/10.1016/j.jmbbm.2013.03.014.

18. Smoljkić, M., J. Vander Sloten, P. Segers, and N. Famaey. Non-invasive, energy-based assessment of patient-specific material properties of arterial tissue. *Biomech. Model. Mechanobiol.* 14(5):1045–1056, 2015. https://doi.org/10.1007/s10237-015-0653-5.

19. Åstrand, H., J. Stålhand, J. Karlsson, M. Karlsson, B. Sonesson, and T. Länne. In vivo estimation of the contribution of elastin and collagen to the mechanical properties in the human abdominal aorta: effect of age and sex. *J. Appl. Physiol.* 110(1):176–187, 2011. https://doi.org/10.1152/japplphysiol.00579.2010.

20. Masson, I., H. Beaussier, P. Boutouyrie, S. Laurent, J. D. Humphrey, and M. Zidi. Carotid artery mechanical properties and stresses quantified using in vivo data from normotensive and hypertensive humans. *Biomech. Model. Mechanobiol.* 10(6):867–882, 2011. https://doi.org/10.1007/s10237-010-0279-6.

21. Minliang, L., L. Liang, and W. Sun. A new inverse method for estimation of in vivo mechanical properties of the aortic wall. *J. Mech. Behav. Biomed. Mater.* 72:148–158, 2017.

22. Rietzschel, E.-R., M. L. De Buyzere, S. Bekaert, P. Segers, D. De Bacquer, L. Cooman, P. Van Damme, P. Cassiman, M. Langlois, P. van Oostveldt, P. Verdonck, G. De Backer, T. C. Gillebert, and Asklepios Investigators. Rationale, design, methods and baseline characteristics of the Asklepios study. *Eur. J. Cardiovasc. Prev. Rehabil.* 14(2):179–191, 2007.

23. Segers, P., S. Rabben, J. De Backer, J. De Sutter, T. Gillebert, L. Van Bortel, and P. Verdonck. Functional analysis of the common carotid artery: relative distension differences over the vessel wall measured in vivo. *J. Hypertens.* 22(5):973–981, 2004.

24. Rabben, S., S. Baerum, V. Sørhus, and H. Torp. Ultrasound-based vessel wall tracking: an auto-correlation technique with RF center frequency estimation. *Ultrasound Med. Biol.* 28(4):507–517, 2002.

25. Vermeersch, S., E. Rietzschel, M. De Buyzere, L. Van Bortel, Y. D'Asseler, T. Gillebert, P. Verdonck, and P. Segers. Validation of a new automated IMT measurement algorithm. *J. Hum. Hypertens.* 21:976–978, 2007.

26. Weisbecker, H., D. M. Pierce, P. Regitnig, and G. A. Holzapfel. Layer-specific damage experiments and modeling of human thoracic and abdominal aortas with non-atherosclerotic intimal thickening. *J. Mech. Behav. Biomed. Mater.* 12:93–106, 2012. https://doi.org/10.1016/j.jmbbm.2012.03.012.

27. Holzapfel, G. A., and R. W. Ogden. Constitutive modelling of arteries. *Proc. R. Soc. Lond. A Math. Phys. Eng. Sci.* 466(2118):1551–1597, 2010. https://doi.org/10.1098/rspa.2010.0058.

28. Smoljkić, M., H. Fehervary, P. Van den Bergh, A. Jorge-Peñas, L. Kluyskens, S. Dymarkowski, P. Verbrugghe, B. Meuris, J. Vander Sloten, and N. Famaey. Biomechanical characterization of ascending aortic aneurysms. *Biomech. Model. Mechanobiol.* 16(2):705–720, 2017.

29. Smoljkić, M., P. Verbrugghe, M. Larsson, E. Widman, H. Fehervary, J. D'hooge, J. Vander Sloten, and N. Famaey. Comparison of in vivo vs. ex situ obtained material properties of sheep common carotid artery. *Med. Eng. Phys.* 55:16–24, 2018.

30. Humphrey, J., J. Eberth, W. Dye, and R. Gleason. Fundamental role of axial stress in compensatory adaptations by arteries. *J. Biomech.* 42:1–8, 2009.

31. Roach, M., and A. Burton. The reason for the shape of the distensibility curves of arteries. *Can. J. Biochem. Physiol.* 35(8):681–690, 1957.

32. Wolinsky, H., and S. Glagov. Structural basis for the static mechanical properties of the aortic media. *Circ. Res.* 14:400–413, 1964.

33. Horný, L., T. Adámek, and M. Kulvajtová. A comparison of age-related changes in axial prestretch in human carotid arteries and in human abdominal aorta. *Biomech. Model. Mechanobiol.* 2016. https://doi.org/10.1007/s10237-016-0797-y.

34. Becker, W., J. Oakley, C. Surace, P. Gili, J. Rowson, and K. Worden. Bayesian sensitivity analysis of a nonlinear finite element model. *Mech. Syst. Signal Process.* 32:18–31, 2012.

35. Kawasaki, T., S. Sasayama, S.-I. Yagi, T. Asakawa, and T. Hirai. Non-invasive assessment of the age related changes in stiffness of major branches of the human arteries. *Cardiovasc. Res.* 21(9):678–687, 1987. https://doi.org/10.1093/cvr/21.9.678.

36. Mitchell, G. F., H. Parise, E. J. Benjamin, M. G. Larson, M. J. Keyes, J. A. Vita, R. S. Vasan, and D. Levy. Changes in arterial stiffness and wave reflection with advancing age in healthy men and women. *Hypertension*. 43(6):1239–1245, 2004. https://doi.org/10.1161/01.HYP.0000128420.01881.aa.

37. Vermeersch, S. J., E. R. Rietzschel, M. L. De Buyzere, D. De Bacquer, G. De Backer, L. M. Van Bortel, T. C. Gillebert, P. R. Verdonck, and P. Segers. Age and gender related patterns in carotid-femoral PWV and carotid and femoral stiffness in a large healthy, middle-aged population. *J. Hypertens.* 26:1411–1419, 2008. https://doi.org/10.1097/HJH.0b013e3282ffac00.

38. Toto-Moukouo, J., A. Achimastos, R. Asmar, C. Hugues, and M. Safar. Pulse wave velocity in patients with obesity and hypertension. *Am. Heart J.* 112(1):136–140, 1986. https://doi.org/10.1016/0002-8703(86)90691-5.

39. Wildman, R. P., R. H. Mackey, A. Bostom, T. Thompson, and K. Sutton-Tyrrell. Measures of obesity are associated with vascular stiffness in young and older adults. *Hypertension*. 42(4):468–473, 2003. https://doi.org/10.1161/01.HYP.0000090360.78539.CD.

40. Zebekakis, P. E., T. Nawrot, L. Thijs, E. J. Balkestein, J. van der Heijden-Spek, L. M. Van Bortel, H. A. Struijker-boudier, M. E. Safar, and J. A. Staessen. Obesity is associated with increased arterial stiffness from adolescence until old age. *J. Hypertens.* 23:1839–1846, 2005.

41. Hollander, M., A. Hak, P. Koudstaal, M. Bots, D. Grobbee, A. Hofman, J. Witteman, and M. Breteler. Comparison

between measures of atherosclerosis and risk of stroke. *Stroke*. 34(10):2367–2372, 2003. https://doi.org/10.1161/01.STR.00000 91393.32060.0E.

42. El Khoudary, S., R. Wildman, K. Matthews, R. Thurston, J. Bromberger, and K. Sutton-Tyrrell. Progression rates of carotid intima-media thickness and adventitial diameter during the menopausal transition. *Menopause*. 20:8–14, 2013. https://doi.org/10.1097/gme.0b013e3182611787.